10 OAM × 16 Wavelengths Two-Layer Switch based on an Integrated Mode Multiplexer for 19.2 Tb/s Data Traffic

M. Scaffardi[(1)], M.N. Malik[(2)], N. Zhang[(3)], P. Rydlichowski[(4)], V. Toccafondo[(1)], C. Klitis[(3)], M. P. J. Lavery[(3)], J. Zhu[(5)], X. Cai[(6)], S. Yu[(7)], G. Preve[(1)], M. Sorel[(3)], A. Bogoni[(1,2)]

***Abstract*—A two-layer switch exploiting orbital angular momentum (OAM) and wavelength of the light as switching domains is presented, aiming to increase the scalability with respect to the single-layer switches. The switch is able to accept 160 optical Gaussian data inputs on a 16-channel wavelength division multiplexing (WDM) grid and direct each input signals to different output ports exploiting 10 OAMs. The optical switch is based on an integrated OAM multiplexer followed by a compact OAM demultiplexer consisting of two refractive elements. Its experimental characterization confirmed a total enabled throughput of 19.2 Tb/s, thanks to the 30 GHz bandwidth available for each port. The switching time can be lower than 1 µs. The OAM switch power consumption, solely due to the thermal tuning of the OAM emitters, since the OAM demux is passive, is 1.35 mW/Gb/s.**

In the proposed switching architecture the number of active components, i.e. the power consumption, scales linear with the number of ports. This is favorable in comparison with single-layer switches that cascade e.g. 2x2 elementary blocks to obtain large port counts, which scale with the square of the number of ports.

The switch accepts input and output signals with Gaussian phase profile that propagate through optical fibers and waveguides, thus making it compatible with standard telecom devices. The suitability of the switch to support real data-traffic is proved by successfully testing it with 10G Ethernet and Fiber Channel over Ethernet (FCoE) data traffic and video traffic. A possible application scenario is represented by a data-center network where the switch can be used to create a low-power consumption network parallel to the network based on standard electronic routers, to manage large traffic flows.

***Index Terms*—Interconnection networks, orbital angular momentum, optical vortex, silicon photonics.**

I. Introduction

The recent years have witnessed a growing data center traffic which, in turn, tends to saturate the capacity of current deployed switches. This also rises issues related to the power consumption and footprint of the switches [1][2][3]. In this scenario, an explored approach to overcome the limitations of the current networking infrastructure is to utilize optical switching-based interconnection networks [4][5][6].

A large number of studies have focused on single-layer optical switches, i.e. exploiting a single switching domain as e.g. space and wavelength. The routing of the signals between switch input and output ports is realized by modifying the physical paths within the switch [7][8][9] or by wavelength tuning [10]. Commercial bulk switches based on micro-3D electro-mechanical systems (MEMS) provides hundreds of ports with large-bandwidth interconnections transparent with respect to the wavelength and the modulation format with hundreds of milliwatts per port power consumption. The reconfiguration time in the range of tens of milliseconds is not suitable for the typical data-center packet switching scenario. Moreover, the footprint is typically large [7] [11].

The integrated technology promises to overcome the reconfiguration time and footprint issues of the aforementioned bulk solutions. The Indium-Phosphide platform switching matrices are demonstrated based on a broadcast and select approach, where semiconductor optical amplifiers (SOAs) are integrated to compensate for the high losses. 16x16 reconfigurable non-blocking switches based on multi-stage architectures are demonstrated [8][12], showing tens of nanoseconds reconfiguration time and a power consumption in the order of Watt per port. The high-losses of the InP waveguides and the high power consumption of the SOAs necessary for the losses compensation hamper the scalability.

Lower power consumption, with fast reconfiguration time, can be obtained with Silicon technology. An 8x8 switch with sub-microsecond switching time is demonstrated in [13] cascading stages based on 2x2 microring resonators switching elements. A 64x64 MEMS switch with planar silicon technology is demonstrated with sub-microsecond switching time, low loss and requiring tens of Volts driving voltage [14]. Switching matrices based on the cascade of 2x2 Mach-Zehnder (MZ) switches are also implemented. A 32x32 ports non-blocking switch is demonstrated with a path-independent insertion loss (PILOSS) architecture based on thermo-optic effect with tens of microsecond switching time, and power consumption of one hundred milliwatts per port [9]. The scalability and performance of these architectures are limited by the number of achieved switch ports and the total achieved throughput.

The authors acknowledge support from the technical staff of the James Watt Nanofabrication Centre at Glasgow University.

[(1)] CNIT, Via Moruzzi 1, 56124 Pisa, Italy, mirco.scaffardi@cnit.it
[(2)] Scuola Superiore Sant'Anna, Via Moruzzi 1, 56124 Pisa, Italy
[(3)] University of Glasgow, Oakfield Avenue, Glasgow G12 8LT, UK
[(4)] Poznan Supercomputing and Networking Center (PSNC), Poznań, Poland
[(5)] Northumbria University, Newcastle upon Tyne NE1 8ST, UK
[(6)] State Key Laboratory of Optoelectronic Materials and Technologies, Sun Yat-sen University, Guangzhou, China)
[(7)] University of Bristol, University Walk, Bristol BS8 1TR, UK

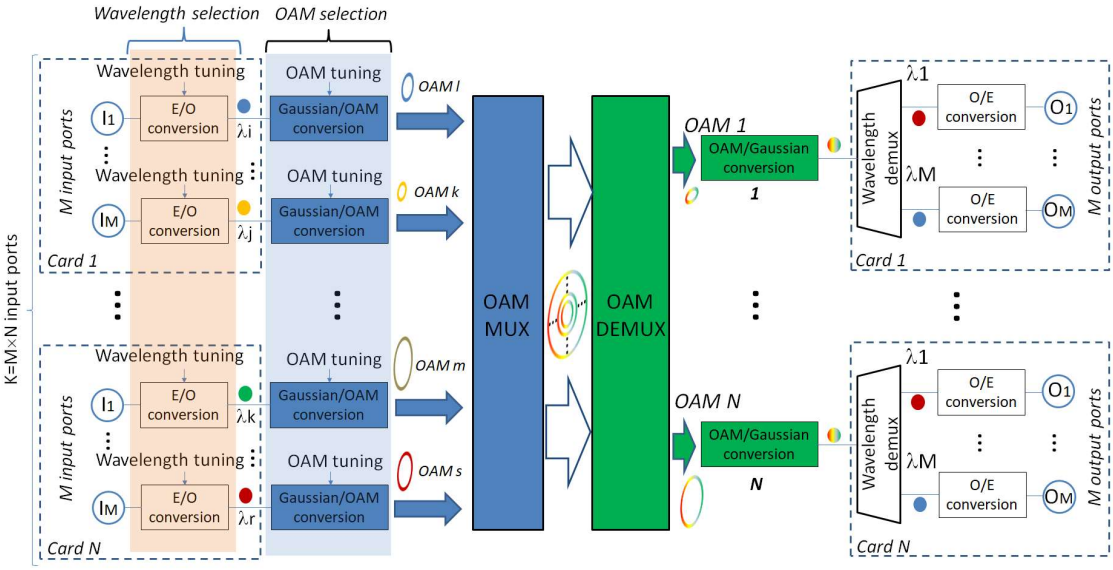

Fig. 1: Working principle of the OAM-wavelength switch for multi-layer interconnection networks.

Besides single-layer switches, a different approach is represented by the multi-layer (or multiplane) switches. Here the output ports are addressed exploiting together multiple domains, as e.g. space, wavelength, time, polarization instead of a single one. Each domain contributes to the routing through a reduced number of physical paths with respect to the single-layer architectures, thus allowing for scalability improvement [15][16]. One of the largest implementation is a two-layer 8x8 switch exploiting space and wavelength domain [17]. In this implementation, SOAs are used as amplifying and selecting elements. We have proposed to exploit the OAM of light as switching domain in conjunction with wavelength to implement two-layer switches [18]. The orthogonality between different OAM modes allows co-propagating beams ideally without crosstalk [19]. Previous demonstrations of OAM switching are demonstrated with bulk implementations based on programmable spatial light modulators for a 2-port switch [20], while integrated solutions are demonstrated not for OAM but for TE modes [21]. In [22] an OAM-wavelength switch exploiting 4 OAM modes and 4 wavelengths was demonstrated with tens of microseconds switching time exploiting an integrated OAM multiplexer with 4 concentric waveguides, which allows for 4 input ports. This switch has been characterized also in a packet switching scenario exploiting a two-step scheduling [23]. In [24] an OAM-wavelength switch with 10 input ports exploiting an integrated OAM multiplexer with 10 concentric emitters is characterized, showing an improved switching time. Performance with real data traffic has been reported briefly in [25].

Here we present a complete characterization of a 10-input ports OAM-wavelength switch, including a scalability analysis and networking considerations regarding the application scenario.

The manuscript is organized as follows. Section II describes the working principle of the two-layer switch. Section III presents the experimental characterization. The testing with real data traffic is presented in Section IV. In Section V the performance of the switch is analyzed followed by the description of the application scenarios in Section VI. The conclusions are drawn in Section VII.

II. Working Principle

The general architecture for the OAM-wavelength switch, presented in [18] for a first implementation without tunable integrated OAM emitters, is shown in Fig.1 and shortly explained in the following. The architecture is composed of N input cards connected to N output cards. Each card has M ports, which gives a total number of $K=N\cdot M$ switch input/output ports. For ease of clarity, the transmitter and receiver sides are presented in the left- and right-hand sides of the figure, respectively.

The cards are addressed by means of N OAM modes, while the ports of each card are addressed by M wavelength channels, in such a way that at each signal present at an input port is assigned a wavelength and is mapped onto an OAM depending on the destination port and card. The wavelength is fixed by electro-optical conversion, while OAM mapping is operated through a beam transformation from Gaussian, the modal distribution typical for fibres and waveguides, to OAM, which needs free-space or special waveguide or fiber to propagate [19], [26]. The OAM beams coming from different ports are spatially multiplexed (OAM mux) and afterwards demultiplexed (OAM demux), being directed to different directions depending on the OAM mode order. OAM to Gaussian conversion and wavelength demultiplexing are the last two steps before the O/E conversion to reach the destination port. The E/O conversion can be implemented with electro-optical modulators, while the conversion of the optical beam from Gaussian mode (Gaussian intensity distribution) to OAM mode (doughnut intensity profile) can be implemented with special integrated waveguides with grating impressed on the inner side wall, [27] [28] [29]. The OAM beam is emitted orthogonal with respect to the waveguide plain, with possibility of OAM tuning by heating. The integration of concentric OAM emitters implements at the same time mode conversion and spatial multiplexing. The multiplexed beam propagates in free-space to reach an OAM demultiplexer realized with an OAM sorter [30] based on two cascaded refractive elements. The spatially separated Gaussian beams can be coupled to

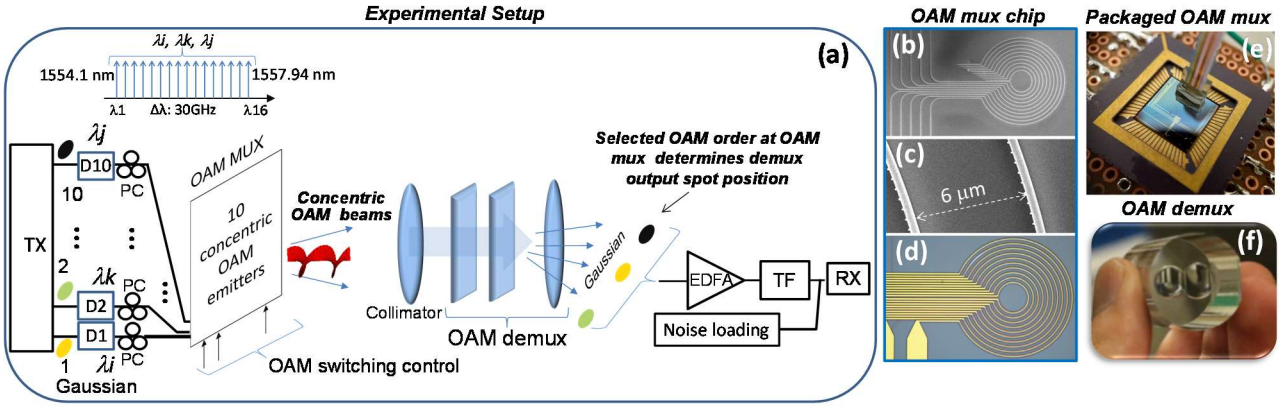

Fig. 2: (a) Experimental setup. Tx: transmitter; Di: fiber delay; PC: polarization controller; EDFA: erbium doped fiber amplifier; TF: tunable filter; Rx: receiver. (b) SEM image of the OAM mux. (c) Magnification of (b) showing the waveguide gratings. (d) Microscope picture of the OAM mux. (e) Integrated OAM multiplexer packaged in ceramic frame with an array of 10 optical fibers and wire bonding. (f) OAM demultiplexer.

standard fiber or integrated waveguide and sent to an arrayed waveguide grating (AWG). Photoreceivers at the output ports can be used to implement O/E conversion. An implementation based on an integrated OAM mux and a compact OAM demux enables small form-factor switching circuits, with size in cube centimeter range.

III. Experimental Setups and Characterization

In this section we report the implementation and the characterization of OAM-wavelength switch exploiting 10 OAM modes and 16 wavelength channels.

A. Experimental Setup

The experimental setup for the characterization of the switch is shown in Fig. 2(a). A set of 10 optical data lines is generated in a transmitter (Tx), operating decorrelation by means of optical delay lines (Di) of different length. The data are generated with OOK and 16QAM modulation formats. The wavelength of each data input line is set to match a comb of 16 wavelengths with 30 GHz spacing as shown at the top of Fig. 2 (a). The data signals are connected to the 10 concentric waveguides of the integrated OAM multiplexer shown in Fig. 2 (b) at the scanning electron microscope (SEM). Each waveguide converts the input Gaussian signal to a free-space OAM beam emitted vertical with respect to the waveguide plain thanks to the grating impressed on the waveguide inner side wall (see Fig. 2 (c)). Since the waveguides are concentric, a set of 10 spatially multiplexed OAM beams is emitted [28]. Polarization controllers (PC) allow optimizing the power coupling into the input waveguides, since the OAM mux works on signals with linear polarization. The emitted OAM beams have an order $l \propto R \cdot n/\lambda$, where R is the radius of the waveguide, n is effective refractive index and λ is the signal wavelength. At a fixed temperature, the order of the emitted OAM beam depends on the input wavelength. Nevertheless, by controlling the refractive index through thermal tuning it is possible to control the order of the emitted beams. OAM modes are selected in the set $l = [1,..,10]$. Fig. 2 (d) shows a microscope image of the OAM mux where the metal wires allowing for the waveguides thermal tuning are visible.

The device is fabricated on a silicon-on-insulator (SOI) wafer with a 220 nm-thick silicon core and a 2 μm of buried oxide, and the out-coupling efficiency is 35%. The OAM mux is packaged in a ceramic chip carrier with bonded electric wires to independently tune the emitted modes. The silicon chip is attached on a 16 mm x 16 mm ceramic leadless chip carrier using an automatic die-attachment machine. It is pigtailed with a 12-channel glass fiber array using an index matching and UV curing epoxy for easy coupling of light into waveguides (see Fig. 2 (e)). The multiplexed OAM beams are forwarded to the OAM demux, realized in a compact way by means of two cascaded diffractive elements (see Fig. 2 (f)) that convert the OAM beams into plane waves with a phase front tilt that depends on the order of the incoming OAM beam [31]. When focused with a lens, the tilted plane waves can be coupled to single mode fibers (SMF) placed at the focal plane of the lens. These are then amplified by an EDFA, filtered (TF) and then received (Rx). A noise-loading stage allows bit error rate (BER) measurements.

B. Characterization Results

The switch is characterized in terms of supported OAM modes and wavelengths channels in order to verify the maximum number of allowed ports. The OAM mux input waveguides are fed one by one with a 30 Gb/s OOK pseudo-random bit sequence (PRBS) 2^{31}-1 mapped on different wavelengths and different OAM modes as explained in the previous sub-section. The BER curves are reported for two extreme wavelengths in the comb λ1=1554.1 nm (Fig. 3(a)) and λ16=1557.94 nm (Fig. 3(b)), for the two worst performing waveguides (3 and 10 numbered from the smallest to the largest) and for the first ($l=1$) and the last ($l=10$) OAM mode. The OSNR penalty with respect to B2B is <1.5 dB at BER=10^{-9}, confirming that the switch can manage up to 16 wavelength x 10 OAM channels, enabling a 160-ports count. The worse performance of waveguide 3 and 10 can be due to imperfections on the inner side wall gratings and to a not efficient fibre-to-waveguide coupling. In terms of crosstalk, a characterization is done by feeding all the switch input ports by the same 20 Gbaud signal at λ1=1554.1 nm. To consider the worst case scenario, the switch is set in a configuration where neighboring waveguides emit consecutive OAM modes and the performance is measured in the central waveguide (7). The switch is tested with 16QAM and OOK data format. Fig. 4 shows the BER vs OSNR for the 16QAM (Fig. 4(a)) and OOK (Fig. 4(b)) in three different cases: i) no crosstalk; ii) crosstalk given by the two adjacent

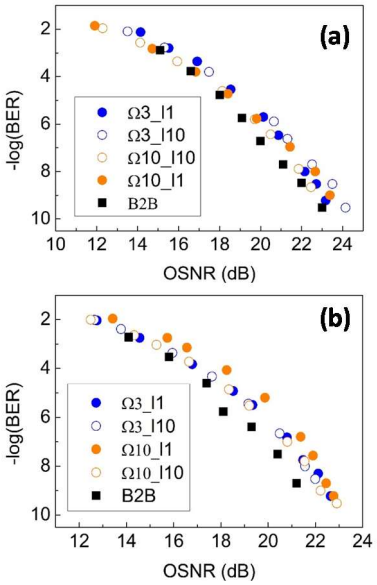

Fig. 3: Two-layer switch tunability characterization. BER vs. OSNR at λ1 (1554.1nm) (a) and λ16 (1557.94nm) (b) for the worst waveguides (Ω3 and Ω10). Waveguides are tuned to emit 10 OAM modes (from *l=1* to *l=10*) for each wavelength channel.

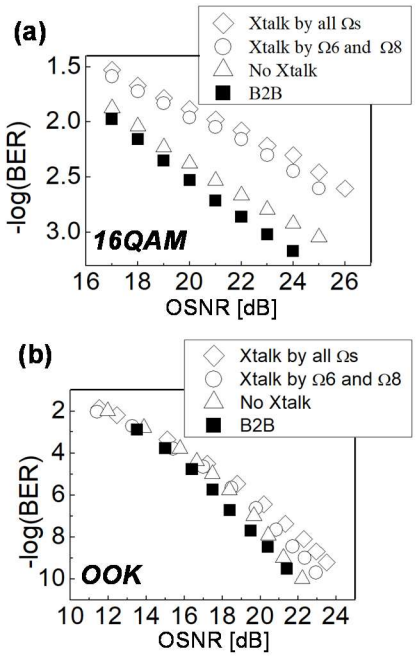

Fig. 4: Crosstalk measurements. BER vs OSNR for OAM emitter 7 in three cases: no crosstalk, crosstalk by Ω6 and Ω8, and crosstalk by all the waveguides. (a) 16QAM input signals. (b) OOK input signals.

waveguides (6 and 8); iii) crosstalk given by all the waveguides. An OSNR penalty < 4 dB at BER $3 \cdot 10^{-3}$ is recorded for 16QAM signals while a penalty < 2.4 dB at BER 10^{-9} is observed for the OOK signals when the crosstalk of all waveguides is considered. The crosstalk arises from both the OAM mux and OAM demux. On the OAM mux side, the beam emitted from each waveguide carries the target OAM mode and, in a small portion of power, also other OAM modes. The purity of the emitted OAM modes, defined as the percentage of power emitted on the target mode with respect to the sum of the spurious power emitted on all the considered set of modes, is higher than 80% [28]. The OAM mux performance can be improved acting on the waveguide geometry, reducing the aperture that brakes the ring shape [28] (Fig. 2 (b), (d)). On the OAM demux side, the crosstalk is due to the not complete spatial separation among the demultiplexed Gaussian spots, which causes coupling of a small portion of power from neighboring spots, coming from OAM modes different from the target one, with the single mode fibre collecting the signal at OAM demux output. This can be overcome by using a lens with longer focal length, thus obtaining larger Gaussian spots spatial separation.

The switching time depends on the tuning time of the waveguides of the integrated OAM mux, based on thermal tuning. The timescale necessary to change from an OAM mode to the following one is about 20 μs [32]. An improvement can be obtained by exploiting an excitation pulse with a voltage 2-times stronger than that required to tune the emitter to a different OAM mode as shown in Fig. 5 (a). This produces a 90% to 10% transition between two consecutive OAM modes in a time as short as 760 ns, as reported in Fig. 5 (b).

IV. Test with Real Data Traffic

The switch capability to operate with real data traffic is investigated exploiting Ethernet data traffic, Fibre Channel over Ethernet (FCoE) data traffic and video traffic. Ethernet and FCoE are commonly used protocols to interconnect servers, blades, machines, in data center environment. In a first experiment, illustrated in Fig. 6, 10G LAN Ethernet traffic is generated with a commercial network traffic generator/analyzer (Spirent N4U). The packet frames have a random length between 64 and 1500 bytes with IPv4 Ethernet traffic payload. The data traffic is converted to the optical domain by a commercial transponder (ADVA FSP300) and sent to the OAM switch. The traffic is sent to the switch input port connected to the seventh OAM mux emitter, which shows the worst performance. The signal wavelength is fixed at 1554.1 nm and the OAM emitter is tuned to emit different modes, i.e. to direct the signal to different output ports. The signal at the switch output is then sent back to the ADVA transponder to be converted to the electrical domain and be received by the network traffic analyzer. In a second experiment FCoE packet frames of 2180 bytes are generated. The performance of the switch are summarized in Table I. No errors are recorded for different switch setting, i.e. different selected OAM modes of the OAM mux emitter, for received power at the input of the ADVA transponder > -16 dBm. By activating the forward error correction (FEC) protocol G.709 of the ADVA transponder, error-free performance is measured for power > -20 dBm. Another experiment is conducted to demonstrate the transmission of video traffic through the switch as shown in Fig. 7. The OAM switch test-bed and ADVA transponder establish an end-to-end 10G LAN connection between server ends. The test-bed runs for 30 minutes without loss of frames, with a latency between the two servers of 0.4 ms as shown from the output messages during the setting up of the connection among the servers reported in Fig. 8.

V. Performance Analysis

A. Bandwidth

The switch bandwidth is limited by the minimum bandwidth among the integrated OAM emitters (OAM mux) and the OAM demultiplexer. The order of the OAM mode generated by each emitter is a decreasing function of the

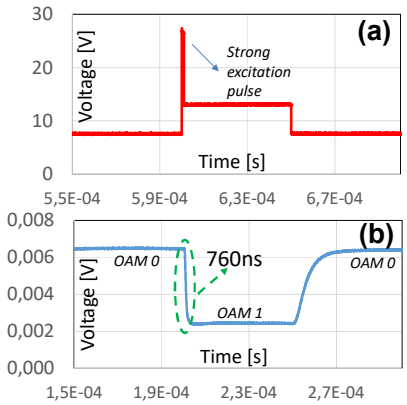

Fig. 5: Switching time measurement. (a) Input control signal. (b) OAM demux output power.

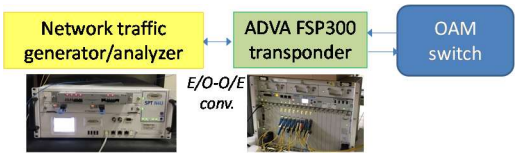

Fig. 6 Setup for OAM switch testing with 10G LAN Ethernet traffic and FCoE traffic.

TABLE I
PERFORMANCE WITH 10G ETHERNET AND FCOE DATA TRAFFIC

Protocol	Switch setting (OAM order)	Transmitted frames	Errors
10G Ethernet	5	909540420	0
10G Ethernet	6	464100381	0
10G Ethernet	7	441714571	0
FCoE	4	173236550	0
FCoE	5	172981299	0
FCoE	6	172738501	0

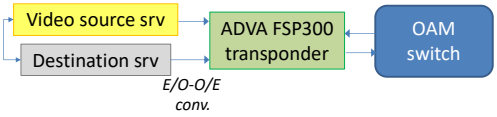

Fig. 7 Setup for OAM switch testing with video traffic. srv: server.

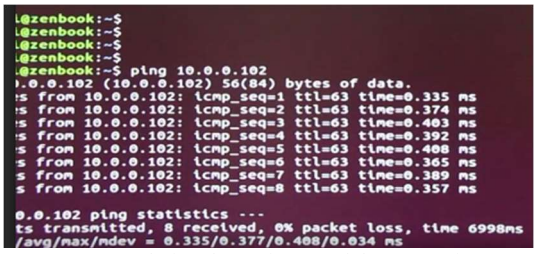

Fig. 8 Output messages during the setting up of the connection among the servers.

wavelength, i.e. the purity of the emitted mode, is not constant within the signal bandwidth, but part of the power is emitted on different modes. From our measurements, a bandwidth of 30 GHz (0.24 nm) allowed to guarantee a mode purity higher than 80% [28]. The OAM demultiplexer instead do not present significant bandwidth limitations since is a completely passive device based on refractive optics. This bandwidth enables transmission at 120 Gb/s with e.g. 16-QAM or 16-PAM modulation.

B. *Scalability*

The total number K of addressable switch ports depends, as explained in the previous paragraphs, by the number of OAM modes N and the number of wavelength channels M supported by the integrated OAM multiplexer and the OAM demultiplexer. The experimental characterization showed that with the current integration technology, a set of N=10 OAM modes tunable over M=16 wavelength channels is possible. This gives the possibility to address K=160 ports. Nevertheless, the number of physical switch input ports corresponds to the number of OAM emitters that can be integrated on a single OAM multiplexer. Each emitter is a waveguide and all the waveguides are concentric. The number of concentric waveguides depends on the minimum separation Δs among the waveguides and maximum waveguide radius R. The thermal isolation represents the main factor influencing the waveguide spacing, since each waveguide must be thermally tunable independently of the neighboring ones. Considering the technology available for the OAM multiplexer, the minimum waveguide spacing is $\Delta s = 6$ µm. With this spacing, when a waveguide is set to emit a target OAM mode, the tuning of any other waveguide over the whole range of 10 OAM modes induces a thermal crosstalk among the waveguides that allows a purity above 80% for the emitted OAM mode.

The maximum radius R is limited by the resolution of the process to write the grating on the inner side wall of the OAM emitter waveguide [28]. The grating forces part of the light travelling into the waveguide to exit. With a uniform grating strength, the intensity emitted in proximity of the waveguide input would be smaller than the intensity emitted in the final part of the waveguide. To ensure uniform emission the grating strength should decrease along the waveguide. This, in turn, requires a high-resolution grating writing process when the radius R becomes large. We demonstrated an integrated multiplexer with up to 10 OAM emitters with 118.95 µm maximum radius [28]. The increase in the number switch ports does not impact on the OAM mux insertion loss, which is determined, for each OAM emitter, by the grating coupler (6 dB) and emission efficiency (4.5 dB). The OAM demux loss is 0.7 dB (85% efficiency) [31] and is not affected by the number of incoming OAM beams to be demultiplexed if the maximum size of the incoming OAM beam, which roughly corresponds to the size of the OAM emitter the beam is generated from, is kept below the OAM demux aperture (8 mm [31]). The number of multiplexed OAM beams, i.e. the number of switch input ports can be increased also resorting to the free-space multiplexing of beams coming from different integrated multiplexers [33].

C. *Power consumption*

The switch power consumption is due to its active elements, i.e. the integrated OAM multiplexer, since the OAM demultiplexer is completely passive. As explained previously, the OAM tuning is obtained by heating the waveguides. The power necessary for the tuning among two consecutive modes is 18 mW. The 10-ports switch demonstrated in this work has a total maximum power consumption of 1.62 W, calculated applying the maximum tuning range for each OAM emitter, which is the worst case scenario.

D. *Comparison with single-layer switch*

The proposed two-layer switch is compared in the following to a high-performance single-layer switch architecture as the one presented in [9], i.e. a switching matrix composed by cascaded 2x2 Mach-Zehnder (MZ) switches

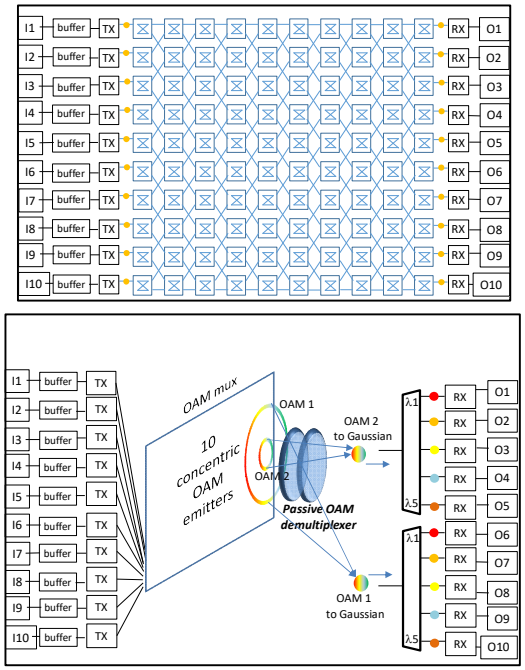

Fig. 9 Top: Single-layer 10-ports switch based on 2x2 Mach-Zhender switches. Bottom: Two-layer 10-ports OAM-wavelength switch.

connected with a path-independent insertion loss (PILOSS) architecture based on thermo-optic effect. This architecture is proved to switch with microsecond timescale, with a power consumption of one hundred milliwatts per port. In this architecture, the number of integrated 2x2 switches scales as the square of the number of ports (K^2). Fig. 9 shows the architecture of a 10-port single-layer switch based on 2x2 Mach-Zhender switches (top) and of a 10-ports two-layer OAM-wavelength switch (bottom). In the two-layer approach, the number of active elements, i.e. the thermally tuned waveguide in the OAM multiplexer, is lower, since it scales as a linear function of the number of ports K and of the number of exploited OAM modes N. A power consumption comparison with the architecture presented in [9] is done for the switching functions, without including the laser and photoreceiver power consumption, since they are the same for both the architectures. The results are shown in Fig. 10. The total power consumption of the OAM-wavelength switch is lower than the one of the silicon MZ-based switch, since it scales with K instead of K^2. The reduction of the number of building block replicas with respect to the MZ-based implementation, can reduce technological issues in terms of fabrication yield, making the solution practicable also for a large number of switch ports. The benefit introduced by the OAM-wavelength approach increases as the number of ports becomes higher. The demonstrated switch performance is summarized in Table II.

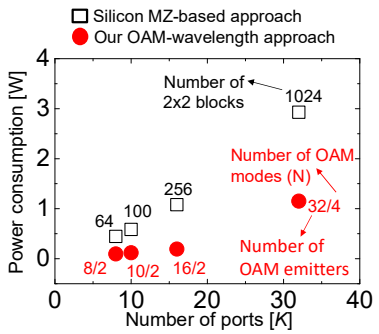

Fig. 10 Power consumption comparison vs. the number of switch ports K

TABLE II
SUMMARY OF THE SWITCH PERFORMANCE

Parameter	Demonstrated	Enabled
Number of ports	10 (10 integrated OAM emitters)	160 (10 OAM modes x 16 wavelength channels
Total capacity	4.8 Tb/s (16QAM, 30Gbaud)	19.2Tb/s (16QAM, 30Gbaud)
Switching time	760ns	
Power consumption	1.35mW/(Gb/s) (16QAM, 30Gbaud)	

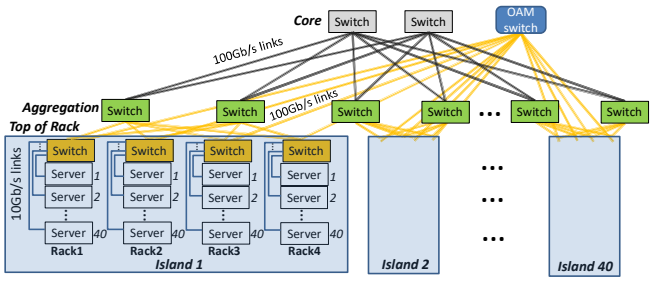

Fig. 11: Possible data center architecture exploiting OAM-wavelength switches in parallel with standard electronic switches. Only part of the racks is displayed for clarity.

VI. Application Scenarios

The two-layer switches can help to overcome the data centers scalability issues. The proposed OAM-wavelength switch could be employed in a data-center network with a typical fat-tree topology as the one shown in Fig. 11. In this use case, the data centre has 40 islands. In each island, there are four racks, each rack with 40 servers. Each server is connected to a top-of-rack (ToR) switch with a 10 Gb/s link. Each ToR is connected to two switches at the aggregation level providing intra-island connectivity as well as links to the core switches. Following an oversubscription approach [34], as it is typically done, the ToR switch is connected to each aggregation-level switch with a 100 Gb/s link. Following the same approach, each aggregation-level switch is also connected to each core-level switch with a 100 Gb/s link. Since the achievable OAM switch reconfiguration time is < 200 ns, the switch can manage data packets of duration of about 2 µs, i.e. about ten times longer than the reconfiguration time. The characterization results showed transmission rates up to 30 Gbaud, i.e. managing up to 120 Gb/s traffic per port with 16QAM modulation. This allows a data transmission speed of 100 Gb/s with suitable FEC. Given this transmission rate, the packet duration is longer than the standard Ethernet traffic, which suggests to exploit the OAM-wavelength switches to create a parallel low-power consumption network to manage large (e.g. elephant [35]) traffic flows. According to the outcomes of the experimental activity, the OAM switch can support up to 160 input/output ports, therefore it can be connected to each ToR switch with an additional link at 100 Gb/s. Therefore, a single OAM-wavelength switch can connect all ToR switches in the 40 islands without passing through the aggregation and core levels.

VII. Conclusion

A two-layer interconnection networks exploiting the OAM of light and wavelength as switching domains is presented. The interconnection network is enabled by a 10-ports OAM

switch composed by the cascade of a silicon integrated OAM multiplexer and a compact OAM demultiplexer based on cascaded refractive elements. Despite OAM switching domain is used, the input and output ports accept and provide, respectively, signals with Gaussian wave front, that propagate through standard optical fibers and waveguides, allowing for the interfacing with commercial telecom equipment. The experimental characterization shows that up to 10 OAM modes and 16 wavelengths are supported, thus enabling 160 ports count. The switch supports 30 GHz bandwidth traffic, thus allowing for a total throughput of 19.2 Tb/s. Extensive testing with 10G Ethernet and Fiber Channel over Ethernet (FCoE) data traffic and video traffic is carried out, showing that the switch can support data center traffic. The demonstrated two-layer switching architecture presents a number of active components that scale linear with respect to the number of ports, differently from single-layer architectures based on 2x2 basic building blocks that scale following a square law. This increases the scalability and reduces the power consumption. The low power consumption (1.62 W) and the switching time lower than 1 µs suggest that the switch could be employed in a data centers network to manage large traffic flows as e.g. elephant traffic, parallel to the network realized with standard electronics switches.

The proposed switch represents one of the few demonstration of two-layer switches and is the first one that employs OAM and wavelength domain with this number of ports. In principle other domains, as e.g. time, could be added in order to further increase the port counts, lowering, at the same time, the scalability requirements for each employed switching domain.

REFERENCES

[1] "Cisco Annual Internet Report", 2020.

[2] J. Shuja et al., "Survey of techniques and architectures for designing energy-efficient data centers," *IEEE Syst. J.*, vol. 10, no. 2, pp. 07–519,Jun. 2016.

[3] A. Ghiasi, "Large data centers interconnect bottlenecks," Opt. Express, Vol. 23, no. 3, p. 2085 (2015).

[4] H. Cho, P. Kapur, and K. C. Saraswat, "Power comparison between high-speed electrical and optical interconnects for interchip communication" *J. Lightw. Technol.*, vol. 22, no. 9, pp. 2021–2033, Sep. 2004.

[5] D. A. B. Miller, "Device requirements for optical interconnects to silicon chips," *Proc. IEEE*, vol. 97, no. 7, pp. 1166–1185, Jul. 2009.

[6] A. Benner, "Cost-effective optics: Enabling the exascale roadmap," in *Proc. 17th IEEE Symp. High Perform. Interconnects*, 2009, pp. 133–137.

[7] Polatis Series 7000 Network Optical Switch. [Online]. Available: http://www.polatis.com/series-7000-384x384-port-software-controlledoptical-circuit-switch-sdn-enabled.asp

[8] A. Wonfor, H. Wang, R. V. Penty, and I. H. White, "Large port count high-speed optical switch fabric for use within datacenters," *IEEE J. Opt. Commun. Netw.*, vol. 3, no. 8, pp. A32–A39, Aug. 2011.

[9] K. Tanizawa *et al.*, "32×32 strictly non-blocking Si-wire optical switch on ultra-small die of 11 × 25 mm2," in *OFC Tech. Dig.*, 2015, Paper M2B.5.

[10] P. Bernasconi, C. Doerr, C. Dragone, M. Cappuzzo, E. Laskowski, A. Paunescu, "Large N×N waveguide grating routers", *J. Lightw. Technol.*, vol. 18, no. 7, pp. 985–991, July. 2000.

[11] [Online]. Available: https://www.diconfiberoptics.com/products/scd0353/SCD-0353A.pdf

[12] R. Stabile, et al., "Monolithic active-passive 16×16 optoelectronic switch", Optics Letters, Vol. 37, no. 22, p. 4666 (2012).

[13] Y. Huang, Q. Cheng, Y.-H. Hung, H. Guan, X. Meng, A. Novack, M. Streshinsky, M. Hochberg, K. Bergman, "Multi-Stage 8×8 Silicon Photonic Switch Based on Dual-Microring Switching Elements", *J. Lightw. Technol.*, vol. 38, no. 2, pp. 194–201, January 2020.

[14] T. J. Seok, et al., "64x64 Low-Loss and Broadband Digital Silicon Photonic MEMS Switches," Proc. ECOC, Tu.1.2.1, Valencia (2015).

[15] R. Gaudino et al., "Can Simple Optical Switching Fabrics Scale to Terabit per Second Switch Capacities?", *J. Opt. Commun. Netw.*, Vol. 1, no. 3, p. B56 (2009).

[16] I. Cerutti et al., "Designing Energy-Efficient Data Center Networks Using Space-Time Optical Interconnection Architectures", IEEE J. Sel. Topics on Quantum Electron., Vol. 19, no. 2, p. 3700209 (2013).

[17] Q. Cheng et al., "First Demonstration of Automated Control and Assessment of a Dynamically Reconfigured Monolithic 8 × 8 Wavelength-and-Space Switch", *J. Opt. Commun. Netw.*,Vol. 7, no. 3, p. A388 (2015).

[18] M. Scaffardi, M. N. Malik, E. Lazzeri , G. Meloni, F. Fresi, L. Poti, N. Andriolli, I. Cerutti, C. Klitis, L. Meriggi, M. Sorel, A. Bogoni, "A Silicon Microring Optical 2x2 Switch Exploiting Orbital Angular Momentum for Interconnection Networks up to 20Gbaud", *IEEE J. Light. Technology*, vol. 35, no. 15, pp. 3142-3148, August 2017.

[19] J. Wang *et al.*, "Terabit free-space data transmission employing orbital angular momentum multiplexing," *Nat. Photon.*, vol. 6, pp. 488–496, 2012.

[20] N. Ahmed, et al., "Reconfigurable 2 × 2 orbital angular momentum based optical switching of 50-Gbaud QPSK channels", Optics Express, Vol. 22, no. 1, p. 756 (2014).

[21] B. Stern et al., "On-chip mode-division multiplexing switch", Optica, Vol. 2, no. 6, p. 530 (2015).

[22] N. Zhang, M. Scaffardi, M. N. Malik, V. Toccafando, C. Kliti, M. P. J. Lavery, G. Meloni, F. Fresi, E. Lazzeri, D. Marini, J. Zhu, X. Cai, S. Yu, L. Poti, G. Preve, A. Bogoni, M. Sorel, "4 OAM x 4 WDM Optical Switching Based on an Innovative Integrated Tunable OAM Multiplexer", Proc. OFC, Th3H.1, San Diego (2018).

[23] M. N. Malik, J. C. Borromeo, M. Scaffardi, F. Scotti, N. Zhang, C. Klitis, M. Lavery, G. Preve, V. Toccafondo, R. Reyes, P. Castoldi, M. Sorel, A. Bogoni, N. Andriolli, "Demonstration of a multiplane OAM-wavelength packet switch controlled by a two-step scheduler implemented in FPGA" *IEEE J. Lightw. Technol*. vol. 37, no. 16 pp. 3948-3955, 2019.

[24] M. N. Malik, N. Zhang, M. Scaffardi, C. Klitis, V. Toccafondo, M. P. J. Lavery, F. Fresi, J.Zhu, X. Cai, S. Yu, L. Potì, G. Preve, M. Sorel, A. Bogoni, "19.2Tb/s Optical Switch Based on an Integrated OAM Multiplexer", Proc. ECOC, We4H.6, Rome (2018).

[25] M. Scaffardi, M.N. Malik, N. Zhang, P. Rydlichowski, V. Toccafondo, C. Klitis, M. P. J. Lavery, J. Zhu, X. Cai, S. Yu, G. Preve, M. Sorel, A. Bogoni, "The Orbital Angular Momentum of Light for Next Generation Optical Switches", Proc ECOC, Tu4E.1, Rome (2018).

[26] J. Zhang, Y. Wen, H. Tan, J. Liu, L. Shen, M. Wang, J. Zhu, C. Guo, Y. Chen, Z. Li, S. Yu , "80-Channel WDM-MDM Transmission over 50-km Ring-Core Fiber Using a Compact OAM DEMUX and Modular 4×4 MIMO Equalization," in *Proc. OFC*, San Diego, USA, 2019, W3F.3.

[27] X. Cai, J. Wang, M. J. Strain, B. Johnson-Morris, J. Zhu, M. Sorel, J. L. O'Brien, Mark G. Thompson, S. Yu, "Integrated Compact Optical Vortex Beam Emitters", *Science*, Vol. 338, Issue 6105, pp. 363-366 (2012).

[28] [Online]. Available: http://arxiv.org/abs/2008.00680.

[29] M. N. Malik, N. Zhang, V. Toccafondo, C. Klitis, M. Lavery, A. Sgambelluri, J. Zhu, X. Cai, S. Yu, G. Preve, M. Sorel, A. Bogoni, M. Scaffardi, "Tunable Orbital Angular Momentum Converter Based on Integrated Multiplexers", *IEEE J. Light. Technology*, 11 September 2020.

[30] G. C. G. Berkhout, M. P. J. Lavery, J. Courtial, M. W. Beijersbergen, M. J. Padgett, "Efficient sorting of orbital angular momentum states of light," *Physical Review Lett*., vol. 105, 153601, Oct. 2010.

[31] M. P. J. Lavery, D. J. Robertson, G. C. G. Berkhout, G. D. Love, M. J. Padgett, and J. Courtial, "Refractive elements for the measurement of the orbital angular momentum of a single photon," *Opt. Express.* vol. 20, pp. 2110-2115, Jan. 2012.

[32] M. J. Strain et al., "Fast electrical switching of orbital angular momentum modes using ultra-compact integrated vortex emitters", Nat. Com., Vol. 5, p. 4856 (2014).

[33] M. Scaffardi et al., "Interconnection network architectures based on integrated orbital angular momentum emitters", Optics Comm., Vol. 408, p. 63 (2018).

[34] Z. Guo, J. Duan, Y. Yang, "Oversubscription Bounded Multicast Scheduling in Fat-tree DataCenter Networks", Proc. 2013 IEEE 27th International Symposium on Parallel & Distributed Processing, pp. 589-600, Boston (2013).

[35] W. Zang, Z. Jing, J. Lan, "An SDN based fast rerouting mechanism for elephant flows in DCN", in Proc. 2017 8th IEEE International Conference on Software Engineering and Service Science, Beijing (2017).